J|A|C|S
COMMUNICATIONS

Published on Web 12/14/2005

Nucleobase Orientation and Ordering in Films of Single-Stranded DNA on Gold

Dmitri Y. Petrovykh,*,†,‡ V. Pérez-Dieste,§ Aric Opdahl,|| Hiromi Kimura-Suda,|| J. M. Sullivan,‡,⊥ Michael J. Tarlov,|| F. J. Himpsel,§ and Lloyd J. Whitman‡

Physics Department, University of Maryland, College Park, Maryland 20742, Naval Research Laboratory, Washington, D.C. 20375, Physics Department, University of Wisconsin, Madison, Wisconsin 53706, National Institute of Standards and Technology, Gaithersburg, Maryland 20899, and Department of Chemistry, Northwestern University, Evanston, Illinois 60208

Received April 14, 2005; E-mail: dmitri.petrovykh@nrl.navy.mil

Understanding the *structure* of single-stranded DNA (ssDNA) immobilized on surfaces is critical for applications exploiting the molecular recognition *function* of nucleic acids.[1] Here we show how the structure of ssDNA monolayers can be characterized using complementary spectroscopies that probe electronic and vibrational states of nucleobases—X-ray photoelectron (XPS), Fourier transform infrared (FTIR), and near-edge X-ray absorption fine structure (NEXAFS) spectroscopies. XPS reveals core-level shifts sensitive to DNA surface chemistry;[2,3] NEXAFS probes electron transitions between core levels and empty valence orbitals that are sensitive to nucleobase orientation;[4,5] and FTIR provides vibrational fingerprints sensitive to orientation and molecular interactions.[3,6]

Existing approaches for using these surface analysis methods to characterize self-assembled monolayers (SAMs) are not directly applicable to studies of ssDNA monolayers, which share very few properties with prototypical SAMs.[1] Whereas van der Waals *attraction* drives the assembly and ordering in typical SAMs, DNA immobilization is subject to strong electrostatic *repulsion*. Strands of ssDNA are also much longer and more flexible than typical molecules in SAMs; therefore, lateral spacing is length-dependent, and long-range lateral ordering is not observed in DNA monolayers. The main type of local ordering that may be present in a DNA film is nucleobase stacking. Nucleobase stacking largely determines the structure and interactions of DNA (including DNA hybridization); therefore, development of methods to detect the associated orientational ordering is a major objective in characterization of DNA films. Such methods will also help to study other biointerfaces (e.g., surface-bound proteins)[1] and to elucidate the correspondence of structures determined ex situ to those in aqueous solutions.

We use thymine homo-oligonucleotides [oligo(dT)] on polycrystalline Au as model ssDNA films to take advantage of analysis methodologies from extensive prior studies.[2,3,6] To examine the effects of attachment chemistry and ssDNA length on immobilization of oligo(dT), we compared monolayers of unmodified $(dT)_5$ (denoted T5 in the Figures) and 5′-thiol-modified $(dT)_5$-SH and $(dT)_{25}$-SH (T5-SH, T25-SH). IR reflection absorption spectra were measured under a dry nitrogen purge using a p-polarized beam at 75° angle of incidence.[3] Normal emission XPS data were acquired in ultrahigh vacuum (UHV) using a monochromatic Al Kα source.[2] NEXAFS data were collected in UHV with a fluorescence yield detector, and p-polarized synchrotron radiation at variable angle of incidence θ_i.[7] See Supporting Information for experimental details.

In Figure 1, we show how the structure and orientation of immobilized ssDNA can be determined from NEXAFS data at the nitrogen X-ray absorption edge. The two major features in these

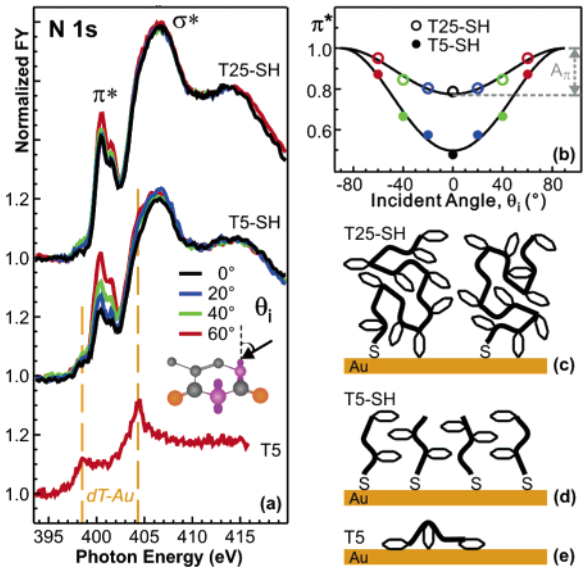

Figure 1. The structure of ssDNA on Au determined using fluorescence yield NEXAFS. (a) The N K-edge spectra of oligo(dT) monolayers on Au. In unmodified $(dT)_5$ films, red-shifted resonances (vertical dashed lines) correspond to dT bases chemisorbed on Au. (b) Polarization dependence of the π^* resonance intensity. A min at $\theta_{min} = 0°$ (p-polarized X-rays normal to the surface, electric field—parallel) indicates that the N π^* orbitals within the nucleobases [(a) inset] are preferentially aligned perpendicular to the surface. (c−e) Structural models of the oligo(dT) monolayers.

nitrogen K-edge spectra of DNA correspond to transitions from N 1s core levels into empty π^* and σ^* orbitals. The spectra in Figure 1a are normalized such that the height of the N π^* peaks above 1 is a semiquantitative measure of the N (and thus the dT *nucleotide*) coverage. In the spectrum of the unmodified $(dT)_5$ film, the π^* and σ^* resonances (vertical dashed lines) are red-shifted,[8] indicating dT chemisorbed on Au (Figure 1e). The two-peak N π^* structure in $(dT)_n$-SH spectra is characteristic of dT nucleobases and likely originates from the two distinct N atoms in dT.[9,10] The orientation of the N π^* orbitals is determined by varying the angle of incidence θ_i of p-polarized X-rays (colors in Figure 1a,b).[4,10−12] The intensity minimum for π^* resonances at normal incidence ($\theta_{min} = 0°$) indicates that dT nucleobases tend to orient parallel to the surface in $(dT)_n$-SH films.[13]

Monolayer structures determined by the complementary XPS and FTIR analysis agree with those determined by NEXAFS (Figure 1c−e). The spectra of $(dT)_5$ monolayers exhibit only features characteristic of dT chemisorbed on Au (vertical dashed lines in Figure 2a−b); that is, corresponding to prone DNA strands (Figure 1e).[3,6] In contrast, the spectra of $(dT)_n$-SH monolayers are dominated by signatures of nonchemisorbed dT; that is, indicating a brush of anchored ssDNA strands (Figure 1c,d).[3]

† University of Maryland.
‡ Naval Research Laboratory.
§ University of Wisconsin.
|| National Institute of Standards and Technology.
⊥ Northwestern University.

10.1021/ja052443e CCC: $33.50

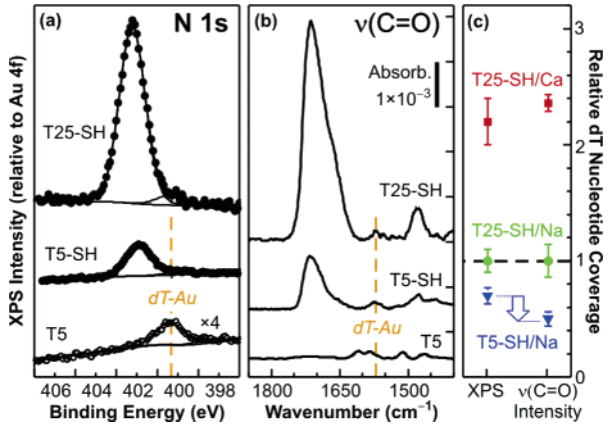

Figure 2. XPS and FTIR characterization of ssDNA on Au. (a) The XPS N 1s intensity normalized by the substrate Au 4f signal. (b) FTIR spectra (peaks ≈ 1700 cm^{-1}) correspond to C═O in dT. Vertical dashed lines in (a and b) indicate features associated with dT chemisorbed on Au. (c) Comparison of relative *nucleotide* coverages determined by XPS and FTIR[2,3] for oligo(dT) deposited from 1 M NaCl and 1 M $CaCl_2$ buffers. The reference *absolute* coverage determined by XPS for T25-SH/Na is 6.3 × 10^{14} dT/cm^2.

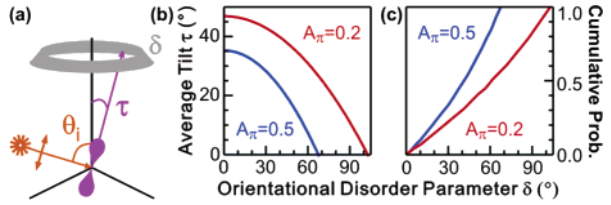

Figure 3. Interpretation of NEXAFS orientation signatures for disordered films. (a) The model assumes that π^* orbitals have random azimuthal orientation and a Gaussian distribution of tilt angles with an *average* tilt τ. The width of this distribution, δ, serves as an orientational disorder parameter; that is, δ is smaller for more ordered systems. The experimental NEXAFS intensity modulation amplitude A_π imposes limits on possible values of τ and δ. Solutions for $A_\pi = 0.2$ and 0.5 (T25-SH and T5-SH in Figure 1b, respectively) are shown in (b), the corresponding cumulative probability distributions for δ are shown in (c). Details in Supporting Information.

The agreement between NEXAFS, XPS, and FTIR on overall film structures provides a basis for comparing respective orientation signatures. Nucleobases can be preferentially oriented by direct interactions with gold only in $(dT)_5$ films which are similar to molecular monolayers. In contrast, $(dT)_n$-SH films more closely resemble multilayers of nucleobases,[14] where intermolecular interactions dominate over interactions with the surface.[10,12] The degree of preferential orientation in $(dT)_n$-SH films can therefore be used to ascertain the presence and to compare the strength of nucleobase interactions in these films.

Molecular orientation is often determined from polarization-dependent modulation of NEXAFS intensity. We augment the standard interpretation[4] of modulation amplitude A_π (Figure 1b) by including effects of orientational disorder, previously shown to be critical in polarization-sensitive spectroscopies.[15] We use the width of a Gaussian distribution of orbital tilt angles as an orientational disorder parameter δ (Figure 3). The standard analysis, which assumes perfect ordering, corresponds to $\delta = 0°$.

For $(dT)_n$-SH films, $\theta_{min} = 0°$, which for orbitals with random azimuthal orientation requires an average tilt $\tau < 55°$. The observed modulation amplitudes A_π further limit the range of τ and δ consistent with the data (Figure 3b,c). Specifically, the narrower range of δ for $(dT)_5$-SH indicates that orientational disorder is significantly lower in films of 5-mers compared to 25-mers (Figure 1c,d).

This difference in orientational disorder is also evident from a comparison of the XPS-determined dT nucleotide coverages and the relative FTIR peak intensities (Figure 2c). NEXAFS and FTIR signals are determined by the same dipole selection rules. In thymine, the N π^* orbitals and carbonyl bonds are roughly orthogonal (Figure 1a inset), so the off-normal *enhancement* of the NEXAFS signal should correlate with a *suppression* of the IR carbonyl peak. XPS is insensitive to molecular orientation, thus for films with similar ordering, the relative FTIR signal correlates with XPS coverage[3]—as shown in Figure 2c for $(dT)_{25}$-SH deposited in NaCl and $CaCl_2$ buffers. In contrast, for $(dT)_5$-SH, the FTIR signal is suppressed by ∼30% relative to the XPS coverage, consistent with preferential orientation of dT bases (Figure 1d).

Preferential orientation of nucleobases in $(dT)_5$-SH monolayers implies correlations between individual bases or, in other words, at least local ordering. This ordering is *not* imposed by direct interactions with Au or by the rigidity of ssDNA backbones. Moreover, hydrogen bonding between oligo(dT) strands is not observed in solution and would not be expected to form during the subsequent rinse in deionized water. Therefore, base stacking is the most likely mechanism of local ordering in $(dT)_5$-SH films.[16] In contrast, the $(dT)_{25}$-SH strands form mostly disordered films similar to polyelectrolyte brushes.[17]

In summary, we demonstrate how the structure, orientation, and ordering in ssDNA monolayers can be quantitatively determined by probing electronic and vibrational states of nucleobases. The simplest interpretation of the agreement between structures observed in UHV and ambient is that both must reflect some aspects of the initial structure in solution. This agreement then strongly suggests that ex situ characterization can be used to study the structure of biosurfaces. This work also establishes a foundation for in situ analysis, as both fluorescence yield NEXAFS and FTIR can be adapted to aqueous environment.

Acknowledgment. D.Y.P. thanks Drs. T.D. Clark and J.N. Russell, Jr. (NRL) for discussions of DNA films. V.P.-D. and F.J.H. thank J.D. Denlinger (ALS) for help with the NEXAFS experiments. Work at NRL was supported by ONR and AFOSR, and at ALS by DOE under Contracts DE-AC03-76SF00098 and DE-FG02-01ER45917.

Supporting Information Available: Materials and Methods; NEXAFS model. This material is available free of charge via the Internet at http://pubs.acs.org.

References

(1) Castner, D. G.; Ratner, B. D. *Surf. Sci.* **2002**, *500*, 28−60.
(2) Petrovykh, D. Y.; Suda, H.; Tarlov, M. J.; Whitman, L. J. *Langmuir* **2004**, *20*, 429−440.
(3) Petrovykh, D. Y.; Kimura-Suda, H.; Whitman, L. J.; Tarlov, M. J. *J. Am. Chem. Soc.* **2003**, *125*, 5219−5226.
(4) Stöhr, J. *NEXAFS Spectroscopy*; Springer-Verlag: Berlin, 1992.
(5) Stöhr, J.; Outka, D. A. *Phys. Rev. B* **1987**, *36*, 7891−7905.
(6) Kimura-Suda, H.; Petrovykh, D. Y.; Tarlov, M. J.; Whitman, L. J. *J. Am. Chem. Soc.* **2003**, *125*, 9014−9015.
(7) Pérez-Dieste, V.; Crain, J. N.; Kirakosian, A.; McChesney, J. L.; Arenholz, E.; Young, A. T.; Denlinger, J. D.; Ederer, D. L.; Callcott, T. A.; Lopez-Rivera, S. A.; Himpsel, F. J. *Phys. Rev. B* **2004**, *70*, 085205.
(8) Both initial state (core-level shift) and final state (metallic screening) effects contribute to the red-shift of resonances for dT chemisorbed on Au.
(9) Kirtley, S. M.; Mullins, O. C.; Chen, J.; Vanelp, J.; George, S. J.; Chen, C. T.; Ohalloran, T.; Cramer, S. P. *Biochim. Biophys. Acta* **1992**, *1132*, 249−254.
(10) Fujii, K.; Akamatsu, K.; Yokoya, A. *J. Phys. Chem. B* **2004**, *108*, 8031−8035.
(11) Crain, J. N.; Kirakosian, A.; Lin, J. L.; Yuedong, G.; Shah, R. R.; Abbott, N. L.; Himpsel, F. J. *J. Appl. Phys.* **2001**, *90*, 3291−3295.
(12) Carravetta, V.; Contini, G.; Plashkevych, O.; Agren, H.; Polzonetti, G. *J. Phys. Chem. A* **1999**, *103*, 4641−4648.
(13) Dipole selection rules allow s−p transitions when the electric field vector is parallel to p-orbitals, which for π^* are normal to planes of nucleobases.
(14) DNA films are *structurally similar* to multilayers of nucleobases, but electrostatic repulsion prevents formation of DNA multilayers in solution.
(15) Simpson, G. J.; Rowlen, K. L. *J. Am. Chem. Soc.* **1999**, *121*, 2635−2636.
(16) The nearest-neighbor distance in a $(dT)_5$-SH film is 1.1 nm (i.e., comparable to that in a DNA duplex), so electrostatic repulsion and entropy may also affect the ordering.
(17) Rant, U.; Arinaga, K.; Fujita, S.; Yokoyama, N.; Abstreiter, G.; Tornow, M. *Langmuir* **2004**, *20*, 10086−10092.

JA052443E

Supporting Information

Nucleobase Orientation and Ordering in Films of Single-Stranded DNA on Gold

Dmitri Y. Petrovykh,*[,†,‡] V. Pérez-Dieste,[§] Aric Opdahl,[‖] Hiromi Kimura-Suda,[‖] J. M. Sullivan,[#,‡] Michael J. Tarlov,[‖] F. J. Himpsel,[§] Lloyd J. Whitman[‡]

[†]*Physics Department, University of Maryland, College Park, MD 20742;* [‡]*Naval Research Laboratory, Washington, DC 20375;* [§]*Physics Department, University of Wisconsin, Madison, WI 53706;* [‖]*National Institute of Standards and Technology, Gaithersburg, MD 2089;* [#]*Department of Chemistry, Northwestern University, Evanston, IL 60208*

**E-mail: dmitri.petrovykh@nrl.navy.mil*

Materials and Methods

Materials. Custom homo-oligonucleotides were synthesized and HPLC purified by the vendors [$(dT)_{25}$-SH from Research Genetics, $(dT)_5$-SH and $(dT)_5$ from IDT] and used as-received without further purification.[a] The 5' alkanethiol modified oligonucleotides [$(dT)_{25}$-SH and $(dT)_5$-SH] were used without removing the protective S-$(CH_2)_6$OH group from the 5' end. Buffer solutions were prepared containing 1 x TE (10 mM Tris-HCl, 1 mM EDTA), 1 M NaCl or 1 M $CaCl_2$, and were adjusted to pH 7 with HCl.

Preparation of DNA Monolayers on Gold Substrates. Polycrystalline gold films on single-crystal Si(100) wafers were used as substrates. Prior to the deposition of gold, the wafers were cleaned using a "piranha solution" consisting of 70% H_2SO_4 and 30% H_2O_2 (30% H_2O_2 in H_2O). Piranha solution must be used with care: it is extremely oxidizing, reacts violently with organics, and should be stored in loosely tightened containers to avoid pressure buildup. After cleaning, a 20 nm Cr adhesion layer was deposited by vapor deposition, followed by 200 nm of Au. Each substrate was again cleaned with piranha solution and rinsed thoroughly with deionized water (18.3 MΩ) immediately prior to adsorption of DNA. Clean gold substrates (≈1 cm^2) were immersed in 2 mL of 1 μM DNA solution in pH 7 buffer solutions at room temperature for 20 h. The DNA concentration was confirmed by UV absorption measurements. For $(dT)_5$ and $(dT)_5$-SH immobilization NaCl was used as the buffer salt. $(dT)_{25}$-SH was immobilized from a $CaCl_2$ buffer to increase the molecular packing density for a closer match with that achieved for $(dT)_5$-SH in NaCl. Additional $(dT)_{25}$-SH films were immobilized from a NaCl buffer to be used as a coverage reference. After deposition, each sample was rinsed with deionized water to remove buffer salt and loosely bound DNA and blown dry under flowing nitrogen.

NEXAFS Measurements. The NEXAFS measurements were done in UHV at the undulator beamline 8.0.1 of the Advanced Light Source. The resolving power of this beamline is better than 8000, providing energy resolution of about 50 meV around the nitrogen K-edge energy range, i.e., less than the intrinsic width of the N 1s core-levels. The custom-built setup for NEXAFS measurements has been previously described in ref 7. Briefly, the measurement chamber allowed the rotation of samples to adjust the (off-normal) angle of incidence θ_i of the p-polarized synchrotron light. The fluorescence yield (FY) signal was detected using a channel plate detector with a detection cone of 40° located at a fixed 45° angle above the incident beam port. We used an Al filter to suppress the background fluorescence from the silicon substrate.

Selective FY detection from the nitrogen K-edge is approximately 10^4 times less efficient than electron yield (EY) detection via the sample current. However, the much more effective background suppression in the FY detection compensates for its lower efficiency. In fact, the FY signal-to-background ratio is approximately an order of magnitude higher than the EY signal-to-background ratio (compare Figure SI1a and SI1b), despite the fact that the EY consisted mainly of high energy Auger electrons, which are more selective than low energy secondaries. It is important to note that the resulting polarization dependence (i.e., the information used to determine orientation and ordering of nucleobases) is essentially identical whether measured with FY or EY detection (Figure SI1c).

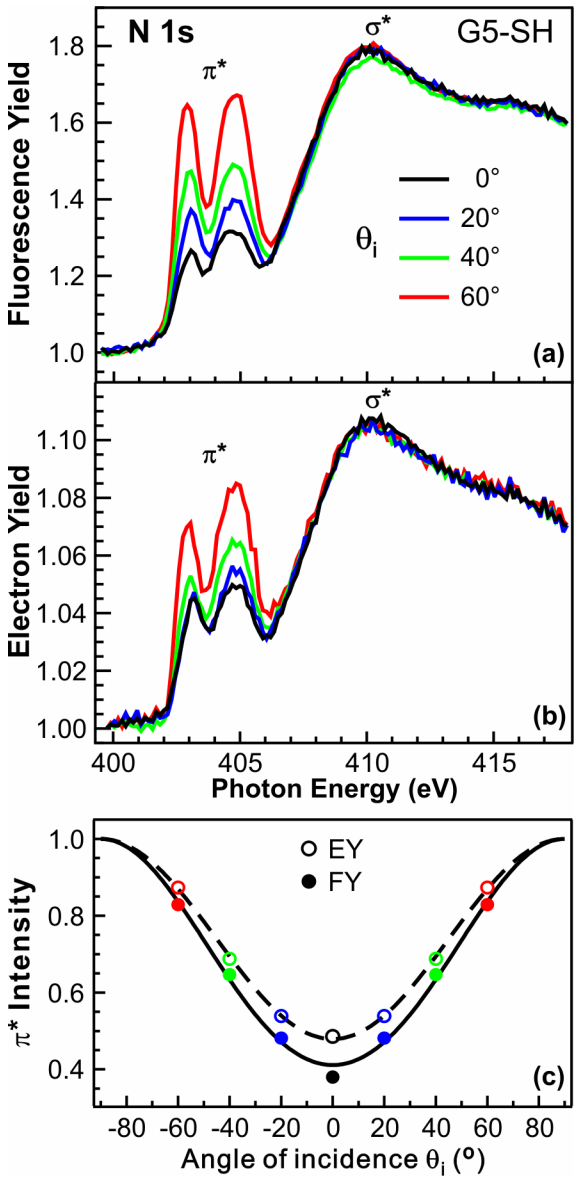

Figure SI1. Comparison of nitrogen K-edge NEXAFS measured with FY and EY detection. The FY (a) and EY (b) spectra were *simultaneously* recorded from a monolayer of $(dG)_5$-SH on Au. The FY detection produced about an order of magnitude higher signal-to-background ratio. (c) The modulation of the π* resonance intensities with the of incidence θ_i (color-coded symbols): FY (black line and full symbols) and EY (dashed line and open symbols).

[a] Certain vendors are identified to adequately specify the experimental procedure. In no case does such identification imply endorsement by the National Institute of Standards and Technology or the Naval Research Laboratory.

An important consideration in establishing the NEXAFS acquisition parameters was minimizing the potential damage to the DNA caused by the incident radiation. As a test of sample degradation, a series of spectra were acquired as a function of sample irradiation time (Figure SI2). Within the first few minutes there was no apparent damage, after 7.5 min of irradiation significant changes in the spectrum occurred. These test spectra were acquired with a photon energy step of 0.2 eV and 2 s per step dwell time. All the data presented in Figure 1a were measured with 0.2 eV photon energy steps, 1 s per step dwell time, and the beam defocused to about 1×3 mm^2 to ensure that exposure remained below the damage threshold. To further minimize sample damage and to test sample uniformity, spectra were measured from 3-4 different spots on each sample for each incidence angle. These multiple scans for each angle were added together for subsequent analysis.

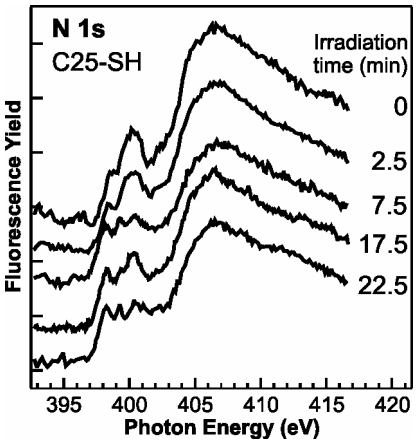

Figure SI2. Monitoring DNA sample damage by exposure to synchrotron radiation. The nitrogen K-edge FY NEXAFS spectra were recorded consecutively from the same spot on a monolayer of $(dC)_{25}$-SH on Au.

NEXAFS data normalization. Various methods can be used to normalize NEXAFS data (ref 4). We use a normalization which produces N π* resonance intensities approximately proportional to the N coverage. Another important feature of this normalization is that normalized peak intensities numerically correspond to peak-to-background ratios, i.e., the most physically appropriate representation of NEXAFS data (ref 4).

First, each FY spectrum was normalized to the photon flux by dividing it by the EY measured simultaneously from a gold mesh. Second, this ratio was multiplied by an angle-dependent factor to achieve a common height of the N-edge jump, i.e., the difference between the pre-edge signal and the continuum states above the near-edge. This makes the signal proportional to the absorption per N atom. Third, the absolute scale was set for each sample by a common scale factor for all angles which was chosen such that the pre-edge background intensity became 1 at θ= 60° (close to the magic angle). The spectra for the other angles were rigidly shifted by a constant to have a pre-edge intensity of 1 as well. This procedure provides a comparison of the absolute N coverage between different samples, assuming that the pre-edge background from the substrate is the same for each sample.

It is well-known that the intensity of σ* resonances is more affected by the uncertainty associated with a specific choice of a background function than the intensity of π* resonances (refs 4,5). It is also known that in aromatic molecules delocalization of molecular orbitals can lead to more complicated relative intensities of π* and σ* resonances than in the case of simple diatomic molecules (refs 4,5). Furthermore, there is strong empirical evidence that in multilayers of aromatic molecules with heteroatom substitutions the apparent polarization-dependence of σ* resonances can be weaker than for π* resonances (refs 10,12). Accordingly, we rely on the polarization dependence of π* rather than σ* resonances to determine orientation and ordering of nucleobases in ssDNA monolayers.

XPS measurements XPS measurements were performed in a commercial UHV system equipped with a monochromatic Al Kα source, a hemispherical electron energy analyzer (58° angle between monochromator and analyzer), and a magnetic electron lens. Detailed descriptions of the quantitative analysis of DNA adsorbed on gold have been presented in refs 2,3. Briefly, normal emission angle-integrated high-resolution scans with 15 eV to 20 eV windows and 20 eV pass energy (0.36 eV nominal analyzer energy resolution) were acquired for Au 4f and 4d, N 1s, P 2p, C 1s, and O 1s core-levels. The reported binding energies (BE) were based on the analyzer energy calibration (Au $4f_{7/2}$ BE = 84.0 eV and Au $4d_{5/2}$ BE = 335.2 eV, for all samples); no charge compensation was necessary. Spectra of the N 1s region were accumulated for 30 min to 60 min, depending on the sample coverage, to obtain an adequate signal-to-noise ratio. The reference Au signals, used to calibrate the photoelectron attenuation and thickness of DNA overlayers, were measured from Au films cleaned by Ar ion sputtering. A convolution of Lorentzian and Gaussian line shapes was used to fit the individual peaks, with typical ratios between 10/90 and 20/80. A linear combination of Shirley and linear functions was used to model the background, with the corresponding coefficients fit simultaneously with the peaks.

FTIR Measurements. IR absorption spectra were obtained using an FTIR spectrometer equipped with a wire grid infrared polarizer (p-polarized) and a variable angle specular reflectance accessory (75° grazing incidence angle). FTIR measurements were performed in a nitrogen purged environment on freshly prepared samples and using a piranha cleaned gold substrate as a reference.

To determine relative dT coverages from FTIR data, ν(C=O) peaks were integrated over the 1600-1850 cm^{-1} range (refs 2,3). The ν(C=O) peaks for $(dT)_5$-SH and $(dT)_{25}$-SH overlap almost perfectly after this normalization.

Model of polarization-dependent NEXAFS. In a NEXAFS experiment orientation and ordering information is obtained by measuring intensities of a π* resonance as a function of the angle of incidence of x-rays θ, e.g., as shown in Figure 1a-b. In general, this π* intensity modulation can be described by two parameters: a modulation amplitude A_π, and an intensity minimum angle θ_{min}. For a fully ordered system the orientation of molecular orbitals can be determined exactly from the polarization-dependence data (refs 4,5).

However, the complexity and flexibility of biological molecules such as ssDNA mean that perfect ordering can no longer be expected and thus should not be assumed in modeling and interpreting the data. In fact, all the caveats noted in the original paper on determination of molecular orientations by NEXAFS apply to ssDNA monolayers: a distribution of π* orbital orientations, apparent tilt angles close to the magic angle, and delocalization of molecular orbitals in aromatic systems (ref 5). Moreover, for a system that contains a distribution of orbital orientations, interpretation of the polarization-dependent measurements in terms of a unique apparent tilt angle in general *will not* result in a value close to the average of that distribution, as has been previously reported for a model of second-harmonic generation (SHG) measurements (ref 15) and as we demonstrate in Figure SI3 for a NEXAFS model described below.

In the dipole approximation, the experimental cross-section for a particular transition is proportional to the square of the dot-product of the polarization vector with the orbital vectors of the π* orbitals

$$I(\theta_i,\omega,\phi) \propto \left[\hat{\varepsilon}(\theta_i)\cdot\hat{O}(\omega,\phi)\right]^2,$$

where $\hat{\varepsilon}$ is the polarization vector of the incident radiation, and $\hat{O}$ is the π* orbital vector described by polar angle ω with respect to the surface normal and azimuthal angle ϕ in the surface plane. We model the total cross-section for the experiment as a statistical average over the contributions from many different orbital orientations. We assume that the orbital vectors have random azimuthal orientation but that the angle they take with respect to the surface normal is distributed according to a Gaussian distribution centered at some preferred tilt angle τ, and with distribution of likely tilt angles given by the width δ (Figure SI3d). The width of the distribution, δ, effectively serves as an orientational disorder parameter in this model. The NEXAFS intensity from such a system excited by an x-ray at an incidence angle θ_i is given by:

$$I_{\text{model}}(\theta_i,\tau,\delta)=\int_0^{2\pi} d\phi \int_0^{\pi} d\omega\, Sin(\omega) P(\omega,\tau,\delta) I(\theta_i,\omega,\phi)\,.$$

$P(\omega,\tau,\delta)$ is a Gaussian distribution normalized over the unit sphere

$$P(\omega,\tau,\delta)=G\left(\frac{\omega-\tau}{\delta}\right)/N(\tau,\delta)\,,$$

where $G(x)=16^{-x^2}$ and with normalization

$$N(\tau,\delta)=\int_0^{2\pi} d\phi \int_0^{\pi} dx\, Sin(x) G\left(\frac{x-\tau}{\delta}\right).$$

Our model agrees with the standard results in the limiting cases where analytical solutions are known (ref 4). Specifically, the standard angular dependence of the NEXAFS intensity is recovered in the *limit of a fixed tilt angle* (δ=0°, red line in Figure SI3b). In the *limit of random orientation*, the total cross-section for the experiment is independent of the incidence angle, as expected.

The purpose of this model is to offer a simple means of *interpreting* experimental NEXAFS data for disordered systems. Accordingly, the *parametrization* of NEXAFS data that we use is exactly the same as that used for the traditional interpretation – the polarization-dependent modulation of NEXAFS intensity is characterized by its amplitude A_π and the position of the intensity minimum θ_{min} (Figures 1b, SI3c).

The behavior of the intensity minimum in our model is identical to that in the standard case of substrates with threefold or higher symmetry (refs 4,5), i.e., the intensity minimum can only occur at an incidence angle θ_{min}=0° or θ_{min}=90° corresponding to an average tilt angle τ <55° or τ >55°, respectively. This bi-valued θ_{min} result is a consequence of integrating orbitals with random azimuthal orientation projected onto a fixed x-ray polarization vector, and is in contrast with the result for a system with fixed tilt and azimuthal angles, for which θ_{min} is uniquely determined by the orientation of the measured orbital.

The main and the only distinction between our analysis and the traditional approach is the *interpretation* of the experimental values of the NEXAFS intensity modulation amplitude A_π (Figures 1b, SI3c). Figure SI3c illustrates the need for such an alternative interpretation – in general the presence or degree of orientational disorder can not be established based on NEXAFS data (open and full symbols) alone, as shown by the essentially identical fits using the standard a+b·sin$^2\theta$ function, which assumes a unique tilt angle (black lines), and our model, which includes disorder (cyan lines). Furthermore, the common assertion that the tilt angle obtained assuming a perfectly uniform system will reflect at least the average value even for a disordered system is actually in general incorrect, e.g., as demonstrated for polarization-dependent SHG in ref 15. For NEXAFS, in Figure SI3a we show that for a fixed average tilt angle τ, the observed intensity modulation amplitude A_π decreases with increasing orientational disorder δ (Cf. Figure 1 in ref 15).

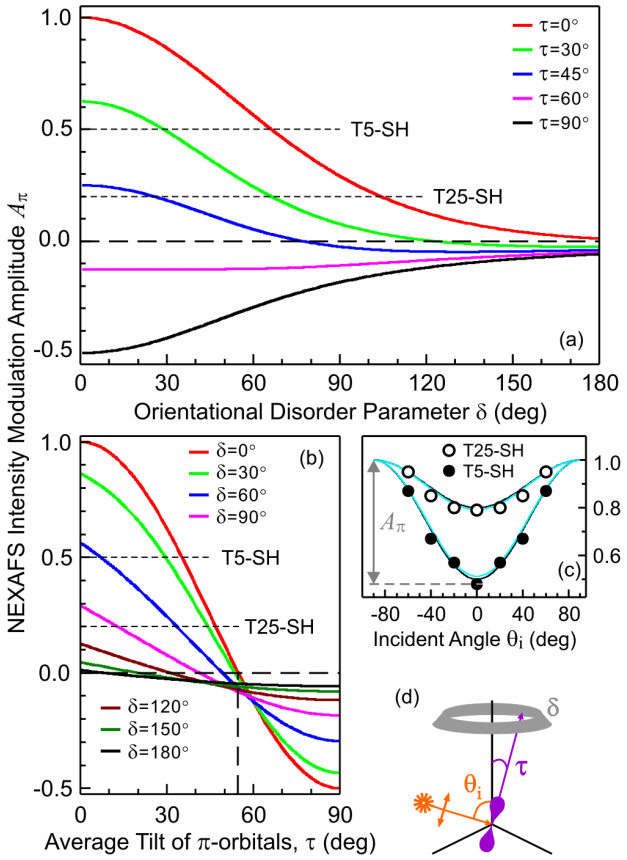

Figure SI3. Modeling the effects of orientational disorder and the average tilt of π-orbitals on the NEXAFS intensity modulation. Polarization-modulation amplitude A_π as a function of: (a) the orientational disorder parameter δ, (b) the average tilt angle τ of π-orbitals. In (a) and (b) colored lines correspond to the indicated discrete values of τ and δ, respectively. (c) Polarization dependence of the π* resonance intensity (symbols = NEXAFS data from Figure 1b). The fits using the model with fixed tilt angle (black line) and the model with disorder (cyan line) are nearly identical. Experimental amplitudes A_π for T5-SH and T25-SH from (c) are indicated in (a) and (b) with dashed lines. (d) Schematic representation of the model parameters: π-orbitals with random azimuthal orientation and a Gaussian distribution of tilt angles, the average tilt angle τ, the width of the distribution δ, and the x-ray angle of incidence θ_i.

The definition of the intensity modulation amplitude A_π that we use in this work is shown in Figure SI3c. The fixed positions of the intensity maxima and minima allow us to simply define A_π as $I(\pi/2,\tau,\delta)-I(0,\tau,\delta)$, such that A_π>0 for τ <55° and A_π<0 for τ >55°, which makes this particular definition convenient for numerical analysis. Other common empirical parametrizations of the standard sine-squared form of polarization-dependent NEXAFS data, e.g., <cos$^2\theta$> or $I(\theta_i$=0°)/$I(\theta_i$=70°), can be readily converted to A_π values via multiplication by an appropriate scaling factor.

In the interpretation commonly used for NEXAFS data from SAMs, a value of a tilt angle is extracted from the measured A_π value assuming a unique correspondence between A_π and τ shown by the red line (δ=0°) in Figure SI3b. Including disorder in the model removes the uniqueness of such correspondence, because a $A_\pi(\tau)$ curve can be calculated for each value of δ; a few representative examples are shown as colored lines in Figure SI3b. Without additional external constraints establishing a unique $A_\pi(\tau)$ correspondence becomes therefore impossible for a system with an unknown degree of orientational disorder.

We can still, however, offer a quantitative probabilistic interpretation of the experimental NEXAFS modulation amplitudes by observing that for each value of A_π only a certain range of possible combinations of the tilt angle, τ and disorder parameter δ will yield model amplitudes consistent with the experimental data. In the graphical representations in Figures SI3a and SI3b this effect is reflected in the fact that only some of the (colored) model curves intersect the horizontal dashed lines corresponding to the experimentally measured A_π values.

The set of solutions that yield the measured amplitude lie along a curve in the $\tau - \delta$ plane which is, to a very high degree of accuracy, parabolic in the disorder parameter, $\tau \approx \tau_o\left(1-\delta^2/\delta_o^2\right)$, where τ_o is the orbital ordering angle for the fully ordered case, and δ_o is the maximum amount of disorder consistent with the experimental data. Values for τ_o and δ_o thus determine all possible solutions which are consistent with the experimental data. One may determine τ_o from the familiar expression for the NEXAFS amplitude for a fully ordered monolayer averaged over all azimuthal orientations, $\mathrm{Sin}^2\left(\tau_o\right) = 2\left(1-A_\pi\right)/3$, where A_π is the measured amplitude. Determining δ_o is more complicated and involves numerical solution based on the model amplitude for $\tau = 0$ shown in Figure SI3a. However, a very accurate estimate is obtained from the analytic form $\delta_o \approx 67.5^\circ\sqrt{Log_2\left(1/A_\pi\right)}$ for amplitudes, A_π, greater than zero. Thus we evaluate $\left(\tau_o, \delta_o\right)$ for the films with NEXAFS amplitudes of 0.5 and 0.2 to be (35.3°,67.5°) and (46.9°,102.8°) respectively and plot the cumulative probability distribution functions in Figure 3c.

Cumulative probability is a natural statistical representation in cases when the direct model prediction is expressed as a limit rather than a specific value (the cumulative probability is defined as the probability that a variable will attain a value less than or equal to each value that the variable can take on). The main advantage of this representation for our model is that a narrower cumulative probability distribution of δ indicates a system with a smaller degree of disorder, i.e., a more ordered system. In general increasing ordering correlates with stronger interactions, thus this approach provides a practical route to determination and comparison of molecular interactions at biointerfaces.

Full References

(1) Castner, D. G.; Ratner, B. D. *Surf. Sci.* **2002**, *500*, 28-60.
(2) Petrovykh, D. Y.; Kimura-Suda, H.; Tarlov, M. J.; Whitman, L. J. *Langmuir* **2004**, *20*, 429-440.
(3) Petrovykh, D. Y.; Kimura-Suda, H.; Whitman, L. J.; Tarlov, M. J. *J. Am. Chem. Soc.* **2003**, *125*, 5219-5226.
(4) Stöhr, J. *NEXAFS Spectroscopy*; Springer-Verlag: Berlin, 1992.
(5) Stöhr, J.; Outka, D. A. *Phys. Rev. B* **1987**, *36*, 7891-7905.
(6) Kimura-Suda, H.; Petrovykh, D. Y.; Tarlov, M. J.; Whitman, L. J. *J. Am. Chem. Soc.* **2003**, *125*, 9014 -9015.
(7) Pérez-Dieste, V.; Crain, J. N.; Kirakosian, A.; McChesney, J. L.; Arenholz, E.; Young, A. T.; Denlinger, J. D.; Ederer, D. L.; Callcott, T. A.; Lopez-Rivera, S. A.; Himpsel, F. J. *Phys. Rev. B* **2004**, *70*, 085205.
(8) Both initial state (core-level shift) and final state (metallic screening) effects contribute to the red-shift of resonances for dT chemisorbed on Au.
(9) Kirtley, S. M.; Mullins, O. C.; Chen, J.; Vanelp, J.; George, S. J.; Chen, C. T.; Ohalloran, T.; Cramer, S. P. *Biochim. Biophys. Acta* **1992**, *1132*, 249-254.
(10) Fujii, K.; Akamatsu, K.; Yokoya, A. *J. Phys. Chem. B* **2004**, *108*, 8031-8035.
(11) Crain, J. N.; Kirakosian, A.; Lin, J. L.; Yuedong, G.; Shah, R. R.; Abbott, N. L.; Himpsel, F. J. *J. Appl. Phys.* **2001**, *90*, 3291-3295.
(12) Carravetta, V.; Contini, G.; Plashkevych, O.; Agren, H.; Polzonetti, G. *J. Phys. Chem. A* **1999**, *103*, 4641-4648.
(13) Dipole selection rules allow s-p transitions when the electric field vector is parallel to p-orbitals, which for π* are normal to planes of nucleobases.
(14) DNA films are *structurally similar* to multilayers of nucleobases, but electrostatic repulsion prevents formation of DNA multilayers in solution.
(15) Simpson, G. J.; Rowlen, K. L. *J. Am. Chem. Soc.* **1999**, *121*, 2635-2636.
(16) The nearest-neighbor distance in a $(dT)_5$-SH film is 1.1 nm (i.e., comparable to that in a DNA duplex), so electrostatic repulsion and entropy may also affect the ordering.
(17) Rant, U.; Arinaga, K.; Fujita, S.; Yokoyama, N.; Abstreiter, G.; Tornow, M. *Langmuir* **2004**, *20*, 10086-10092.